

Fluorinated Star-Shaped Block Copolymers: Synthesis and Optical Properties

Jing Qu, Xinran Luo, Zhonggang Wang

Department of Polymer Science and Materials, School of Chemical Engineering, Dalian University of Technology, Dalian 116024, China

Correspondence to: Z. Wang (E-mail: zgwang@dlut.edu.cn)

Received 1 December 2015; accepted 10 January 2016; published online 8 February 2016

DOI: 10.1002/pola.28056

ABSTRACT: Tetrakis(4-(1-bromoethyl)phenyl)silane is synthesized and utilized to initiate the atom transfer radical polymerization (ATRP) of methyl methacrylate (MMA) to generate bromo-terminated four-armed PMMA macroinitiators, which further initiate the ATRP of methylacryloyloxy-2-hydroxypropyl perfluorooctanoate (FGOA) to create fluorinated star-shaped block copolymers PMMA-*b*-poly(FGOA)s with fluorine content ranging from 0 to 31.7 wt %. The polymerizations are well controlled with the polydispersity indices <1.30. The polymers readily dissolve in common organic solvents and show good film-formation. Compared with the nonfluorinated sample, the fluorinated films exhibit significantly increased water contact angles owing to the enrichment of fluorine on the surface. The

enhanced hydrophobicity is advantageous for the optical stability when the devices work under a moist environment. Moreover, the films possess high thermo-optic coefficients, tunable refractive indices, and extremely low birefringence coefficients because of the presence of bulky and rigid tetraphenylsilane core and star-shaped topological structure, showing potential application in optical waveguide devices. © 2016 Wiley Periodicals, Inc. *J. Polym. Sci., Part A: Polym. Chem.* **2016**, *54*, 1969–1977

KEYWORDS: atom transfer radical polymerization; block copolymer; fluorinated; optical property; star polymer

INTRODUCTION Star-shaped polymers are a new class of special macromolecules attracting great attention because of their fascinating topological architecture with multiple chains stretching out from a single core,^{1–7} and some of them have exhibited promising applications in passive optical waveguide materials,⁸ microelectronic devices,⁹ biomedical materials,^{10,11} solid-state Lithium-Ion battery,¹² and so on. Different from conventional branched or hyper-branched polymers with many branches randomly linking to the polymer backbone, star-shaped polymers have regularly branched structure, well-controlled molecular weight, and narrow molecular weight distribution achieved by means of living radical polymerization,^{4,13,14} living anionic polymerization,¹⁵ living cationic polymerization,¹⁶ and “click” chemistry¹⁷ techniques though various synthetic strategies, including core-first, arm-first and the mixed use of the two methods.^{18,19} Relatively, the core-first approach has apparent advantage since, in this way, the multifunctional core compound initiates the polymerization of monomers to generate arms, so the number of arms are conducive to be predefined.

In comparison with the linear polymers of the same molar mass, the peculiar topological architecture of star-shaped polymers leads to a low hydrodynamic volume, small mean

gyration radius, excellent solubility and low viscosity^{2,5,7} as well as low optical birefringence since the star-shaped topology can effectively inhibit the crystallinity and orientation of segments. Especially, the narrow molecular weight distribution are of great advantage in reducing the line width roughness and line edge roughness of small features for the fabrication of optical waveguide devices.⁸

However, for optical waveguide devices, the optical stability of the polymer layer under the humid service condition has been always great concern because the absorbed water will greatly alter refractive index and increase optical transmission loss.^{20–23} It is well known that fluoropolymers possess low surface energy and high hydrophobicity,²⁴ but most fluoropolymers have poor solubility in common organic solvents. Moreover, some perfluoropolymers and their copolymers are conducive to crystallize, resulting in opacity, optical anisotropy, and large birefringence.²⁵ In this regard, the design and synthesis of star-shaped fluorinated polymers provide us the possibility to create new optical materials with the combination of favorable merits of star-shaped polymers and fluoropolymers to fulfill the stringent requirements of optical materials.

Additional Supporting Information may be found in the online version of this article.

© 2016 Wiley Periodicals, Inc.

Based on the above considerations, the present work was undertaken to synthesize a new tetrafunctional compound tetrakis(4-(1-bromoethyl)phenyl)silane (BTES). Using BTES as an initiator, the two-step atom transfer radical polymerization (ATRP) of methyl methacrylate (MMA) and methylacryloyloxyl-2-hydroxypropyl perfluorooctanoate (FGOA) leads to a series of novel star-shaped fluorinated block copolymers with fluorine contents over a wide range from 0 to 31.7 wt%. The fluorinated films are expected to have excellent resistance to moisture, while the incorporation of bulky and rigid tetraphenylsilane core can reduce the orientation degree of segments, and therefore is expected to greatly decrease the birefringence of polymer films. The synthesis and characterization of BTES initiator, star-shaped PMMA macroinitiators and fluorinated star-shaped block copolymers PMMA-*b*-poly(FGOA)s as well as the influence of star-topology and fluorine content on hydrophobicity, surface morphology, and optical properties of fluorinated copolymer films are studied in detail.

EXPERIMENTAL

Materials

Tetrachlorosilane (SiCl₄), *p*-bromoethylbenzene, *n*-butyl lithium, and perfluorooctanoic acid (PFOA) were purchased from J&K-Chemical and used without further purification. Diethyl ether was purified by refluxing over sodium with the indicator benzophenone complex. Carbon tetrachloride and *N,N*-dimethylformamide (DMF) were from Fuyu Fine Chemical Industry and were purified by reduced pressure distillation prior to use. MMA purchased from Tianjin Guangfu Fine Chemical was washed with 5% aqueous NaOH solution to remove the inhibitor, and then washed with distilled water, dried over CaCl₂, and distilled twice over CaH₂ under reduced pressure before use. *N,N,N',N''*-pentamethyldiethylenetriamine (PMDETA) was purchased from Aldrich and used as received. Copper (I) bromide (CuBr) provided by Sinopharm Chemical Reagent was purified by stirring overnight over CH₃COOH at room temperature followed by washing the solid with ethanol before drying at 40 °C *in vacuo* for 1 day. Glycidyl methacrylate (GMA) was from Guangzhou Yuanmao Chemical Corp. Benzoyl peroxide from Sinopharm Chemical Reagent was recrystallized with chloroform and methanol. FGOA was prepared by reacting PFOA with GMA according to the procedure described in our previous article.²⁶ Other chemical reagents are of reagent grade and used as received.

Synthesis of Tetrakis(4-ethylphenyl)silane (TES)

A solution of 32.0 g *p*-bromoethylbenzene (163.6 mmol) in anhydrous diethyl ether (70 mL) was stirred at -78 °C under dry N₂ and treated with 65.5 mL solution of *n*-butyllithium (2.5 M in hexane, 164 mmol) added dropwise over 1 h. The resulting mixture was stirred at -78 °C for 0.5 h, and then 4.70 mL SiCl₄ (40.93 mmol) in 20 mL diethyl ether was added. The mixture was stirred at room temperature overnight; 40 mL 1 N aqueous HCl was added cautiously into the system to stop the reaction. The solvent was removed by rotary evaporation,

and the crude product was washed with deionized water and methanol. Further purification was carried out by recrystallization in toluene to yield white crystals. Yield: 75%. FTIR (KBr, cm⁻¹): 3068 and 3015 (arom. C—H), 2956, 2923, and 2853 (aliph. C—H), 1597 and 1499 (arom. C=C), 1439, 1107, and 732 (Si—C). ¹H NMR (400 MHz, CDCl₃/tetramethylsilane (TMS), ppm): δ 7.5–7.44 (d, 8H), 7.23–7.16 (d, 8H), 2.72–2.60 (q, 8H), 1.30–1.19 (t, 12H). ¹³C NMR (400 MHz, CDCl₃/TMS, ppm): δ 145, 137, 132, 127, 29, 15.

Synthesis of BTES

TES (1.545 mmol; 0.69 g), 1.1 g *N*-bromosuccinimide (6.18 mmol), 0.011 g benzoyl peroxide (0.045 mmol), and 50 mL CCl₄ were charged into a 250 mL three-neck flask equipped with a thermometer, a mechanical stirrer, and condenser under nitrogen atmosphere. The system was heated to the refluxing temperature, and reacted at this temperature for 6 h. After cooling to room temperature, the mixture was filtered and the filtrate was concentrated by vacuum distillation. The resulting solid was purified by recrystallization twice in mixed solvent of toluene and *n*-hexane to give white crystals. Yield 47%. Elemental analysis: calculated for C₃₂H₃₂Br₄Si, C 50.29%, H 4.22%; found, C 50.36%, H 4.29%. IR (KBr, cm⁻¹): 3068 and 3015 (C—H arom.), 2958, 2924, and 2856 (C—H aliph.), 1598 and 1499 (C=C arom.), 1439, 1107, and 732 (Si—C), 1261 and 592 (—C—Br). ¹H NMR (400 MHz, CDCl₃/TMS, ppm): 7.57–7.48 (d, 8H), 7.48–7.41 (d, 8H), 5.26–5.16 (q, 4H), 2.10–1.98 (d, 12H). ¹³C NMR (400 MHz, CDCl₃/TMS, ppm): δ 145, 137, 134, 126, 49, 27.

Synthesis of Star-Shaped PMMA Macroinitiators

The 50 mL Schlenk flask was flame-dried under vacuum prior to use, which was degassed under vacuum at room temperature and back-filled with nitrogen three times. The freshly distilled MMA and DMF were deoxygenated by purging with nitrogen for 1 h, respectively. Then, 38.2 mg BTES (0.05 mmol), 69.3 mg PMDETA (0.4 mmol), 28.7 g CuBr (0.2 mmol), 2 g MMA (20 mmol), and 20 mL DMF were added. The feed molar ratio of BTES:CuBr:PMDETA:MMA is 1:4:8:400. The system was sealed and then degassed three times by freezing and thawing. The polymerizations were conducted at 30 °C under nitrogen atmosphere for 300, 150, 130, and 30 min to obtain four bromo-terminated macroinitiators PMMA-1, PMMA-2, PMMA-3, and PMMA-4, respectively. After cooling to room temperature, the polymerization was stopped by exposing the system to air. The solution was diluted with acetone and passed a neutral alumina column to remove the catalyst, and then precipitated in methanol and dried at 80 °C under vacuum to obtain white solid.

Synthesis of Fluorinated Star-Shaped Block Copolymers

Four-armed star-shaped fluorinated block copolymers were synthesized from fluorinated monomer FGOA using the bromo-terminated star-shaped PMMA macroinitiator by ATRP with a molar ratio of bromo-terminated polymer: CuBr:PMDETA = 1 : 4 : 8. The four block copolymers were prepared in the similar procedure, so only the synthesis of FPMMA-1 is described here as an example. 0.326 g FGOA

(0.59 mmol), 0.618 g PMMA-1 (0.10 mmol), 0.0143 g CuBr (0.10 mmol), and 0.347 g PMDETA (0.20 mmol) and 10 mL DMF were added in a predried Schlenk flask. The polymerization was carried out at 30 °C for 72 h. After cooled to room temperature and exposed the catalyst to air, the reaction mixture was diluted with acetone and passed through a column of neutral alumina to remove the catalyst. The filtrate was concentrated under reduced pressure and then precipitated in excess methanol. After filtered, the solid was washed with diethyl ether repeatedly to remove the possible unreacted FGOA monomer. The product was dried at 80 °C under vacuum to constant weight.

Preparation of Polymer Films

The films of fluorinated star-shaped block copolymers were prepared from their 20 wt % DMF solutions, which were filtered through a 0.22-mm Teflon filter and spin coated onto a silicon wafer. The resulting films were dried at 60 °C for 0.5 h and 120 °C for 4 h to remove the residual solvent under vacuum.

Measurements

Fourier transform infrared spectra (FTIR) were recorded using a Nicolet 20XB FTIR spectrophotometer in the 400–4000 cm^{-1} region. Samples were prepared by dispersing the complexes in KBr and compressing the mixtures to form disks. Sixty-four scans were signal-averaged with a resolution of 2 cm^{-1} at room temperature. ^1H and ^{13}C NMR spectra were carried out by an INOVA-400 NMR spectrometer (Varian) using DCCl_3 or acetone- d_6 as solvent, and TMS as internal standard. Elemental analyses were determined with an Elementar Vario EL III elemental analyzer. Gel permeation chromatography (GPC) analyses were carried out on a PL-GPC220 system using polystyrene (PS) as standard and tetrahydrofuran (THF) as the eluent. DSC curves were measured by a NETZCH DSC 204 thermal analyzer using N_2 as a purge gas (20 mL/min) at a heating rate of 10 °C/min. About 5–10 mg sample was put into the aluminum pan for DSC measurement. XPS measurements were performed in both survey and high resolution mode on a Thermo ESCALAB 250, with a Monochromatic Al K α ($h\nu = 1486.6$ eV) X-ray light source of 150 W at 15 kV. Spectra were acquired at a takeoff angle of 0°, which is defined as the angle between the sample surface normal and the optical axis of the photoelectron spectrometer. The survey spectra from 0 to 1000 eV were collected with a pass energy of 50 eV, while C_{1s} , F_{1s} , and O_{1s} high resolution spectra were acquired with a pass energy of 20 eV. The atomic force microscopy (AFM) images were recorded with a PicoPlus II microscope (Agilent) at room temperature in tapping mode. Contact angles of deionized water were measured on an OCAH200 contact angle goniometer (Dataphysics) at room temperature. For each sample, two films were used for contact angle measurements; 3–4 drops on different position for one sheet were tested, and the obtained values were averaged. The standard deviation of contact angle was found to be within $\pm 2^\circ$. Refractive index and birefringence were measured at room temperature on a Sairon SPA-4000 prism coupler with a gad-

olinium gallium garnet prism. For each sample, at least three pieces of films were measured and their values were averaged. The refractive indices n_{TE} and n_{TM} for the transverse electric (TE) and transverse magnetic (TM) modes of the films were measured by using a Sairon SPA-4000 prism coupler at the wavelengths of 1310 and 1550 nm, respectively, with the accuracy of 0.001 and the resolution of ± 0.0005 . The birefringences (Δn) were calculated as the difference between n_{TE} and n_{TM} . The curves of refractive index as a function of temperature were obtained by measuring the refractive indices at different sample temperatures from 25 to 85 °C. Their slopes are thermo-optic coefficients.

RESULTS AND DISCUSSION

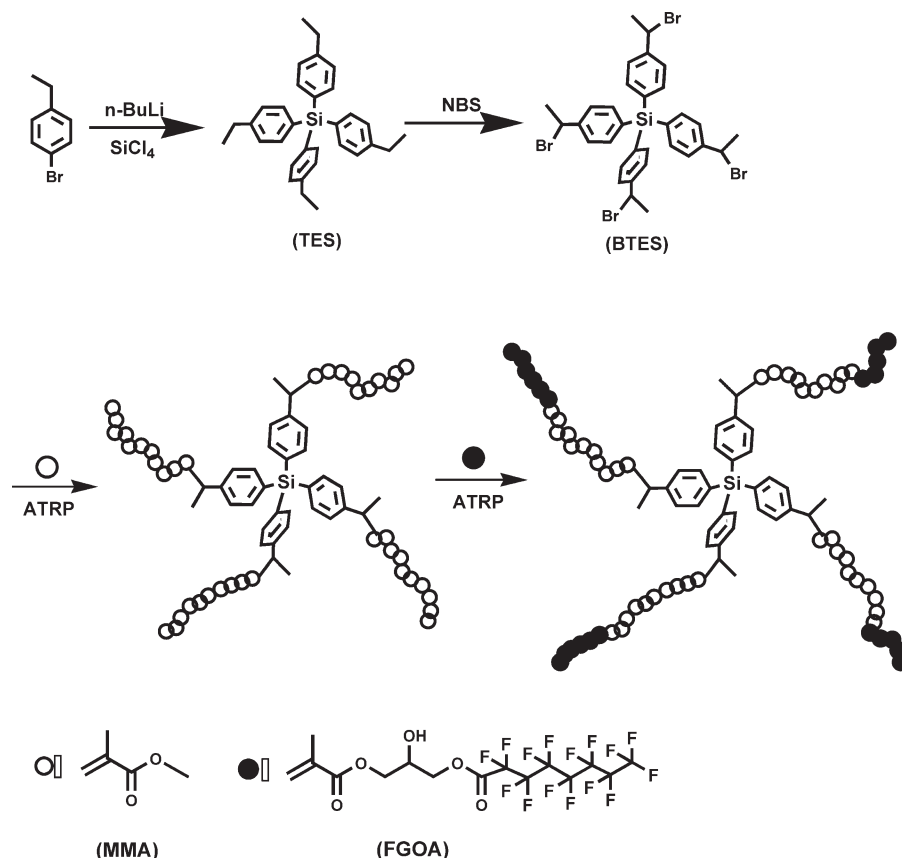
Synthesis and Characterization of Tetrafunctional Initiator (BTES)

As shown in Scheme 1, the designed initiator (BTES) contains a wholly aromatic tetraphenylsilane core. The σ - π conjugation between the electron-deficient silicon atom and benzene ring results in a electron-withdrawing effect on the halogenated α -carbon, which is advantageous for the activation of initiator for ATRP polymerization. Specifically, *p*-bromomethylbenzene was lithiated by *n*-butyllithium, and then reacted with SiCl_4 via nucleophilic reaction to yield TES. The bromination of TES by *N*-bromosuccinimide gave the target tetraphenylsilane-based tetrafunctional initiator (BTES).

The chemical structures of BTES and its precursor TES were confirmed by FTIR, ^1H NMR and ^{13}C NMR spectroscopy. In the FTIR spectra (Fig. S1, Supporting Information), the absorptions at 1439, 1107, and 732 cm^{-1} are characteristics of the C—Si bond in tetraphenylsilane core. The bands at 2800–2960 cm^{-1} are attributed to aliphatic C—H bonds. For BTES, the stretching vibrations of C—Br at 1261 and 592 cm^{-1} indicates the occurrence of bromination reaction.^{27,28} In the ^1H NMR spectrum of TES (Fig. 1), the signals of two protons in benzene ring appear at 7.46–7.16 ppm, whereas the peaks at 2.66 and 1.26 ppm are assigned to the protons of — CH_2 — and — CH_3 groups, respectively. After bromination, the chemical shifts of protons in benzene ring move to 7.57–7.41 ppm, and the protons of — CHBr — and — CH_3 groups appear at 5.21 and 2.04 ppm, respectively. The ^{13}C NMR spectra of TES and BTES (Fig. S2, Supporting Information) reveal that, compared with TES, after bromination, the former signals belonging to the ethyl carbon at 29 and 15 ppm shift to 49 and 27 ppm, respectively.

Synthesis and Characterization of Star-Shaped PMMA Macroinitiators

The bromo-terminated star-shaped PMMA macroinitiators with different molecular weights were prepared in DMF at 30 °C using BTES as an initiator, CuBr and PMDETA as catalysts. The polymerizations were carried out at a relatively low temperature to avoid the self-polymerization of MMA.²⁹ The four PMMA macroinitiators with incremental molecular weights obtained with the polymerization time of 300, 150,



SCHEME 1 Synthesis routes to tetakis(4-(1-bromoethyl)phenyl)silane (BTES), star-shaped PMMA macroinitiators and fluorinated block copolymers.

130, and 30 min are named as PMMA-1, PMMA-2, PMMA-3, and PMMA-4, respectively.

The representative FTIR spectrum of PMMA-4 is presented in Fig. S3 (Supporting Information). Besides the absorptions of Si–C bond and phenyl groups derived from BTES, the

characteristic bands of PMMA chains can be found. For example, the absorptions at $2996\text{--}2850\text{ cm}^{-1}$ are associated to the methyl and methylene groups, while the strong peak at 1732 cm^{-1} corresponds to the carbonyl stretching vibration of ester group. The ^1H NMR spectrum of PMMA-4 is shown in Figure 2. The weak peaks of phenyl protons of tetraphenylsilane core are found at around 7.57 ppm and 7.48 ppm. The peaks at around 1.25–0.75 ppm and 2.02–1.75 ppm are corresponded to the protons of methyl and methylene groups of PMMA backbone, respectively. The methyl protons of COOCH_3 locate at 3.59 ppm.

The number averaged polymerization degree of each PMMA arm (DP_n) and the number average molecular weights (M_n) of four-armed PMMA macroinitiators are calculated from the peak areas of COOCH_3 and phenyl according to eqs 1 and 2, respectively.

$$\text{DP}_n(\text{NMR}) = \frac{A_{\text{COOCH}_3}/3}{A_{\text{phenyl}}/4} \quad (1)$$

$$M_n(\text{NMR}) = 4 \times 100.12 \times \text{DP}_n + 764.30 \quad (2)$$

where A_{COOCH_3} and A_{phenyl} are the peak areas of COOCH_3 and phenyl, respectively; 100.12 is the molecular weight of MMA unit, whereas 764.30 is the molecular weight of BTES core. The data of DP_n and M_n calculated from the ^1H NMR spectra

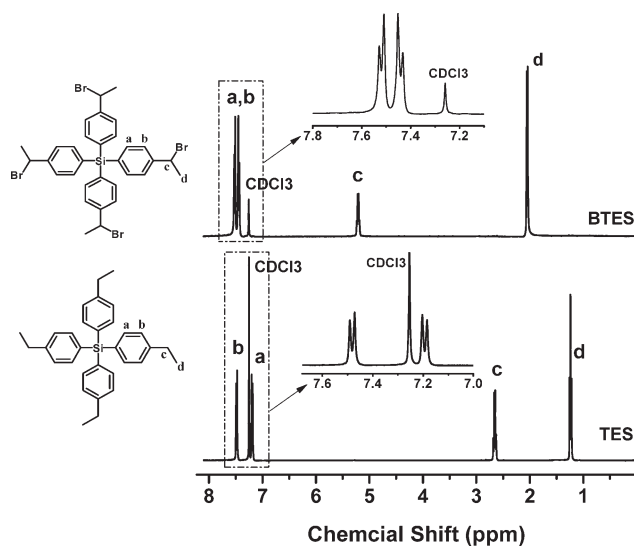


FIGURE 1 ^1H NMR spectra of initiator BTES and its precursor TES.

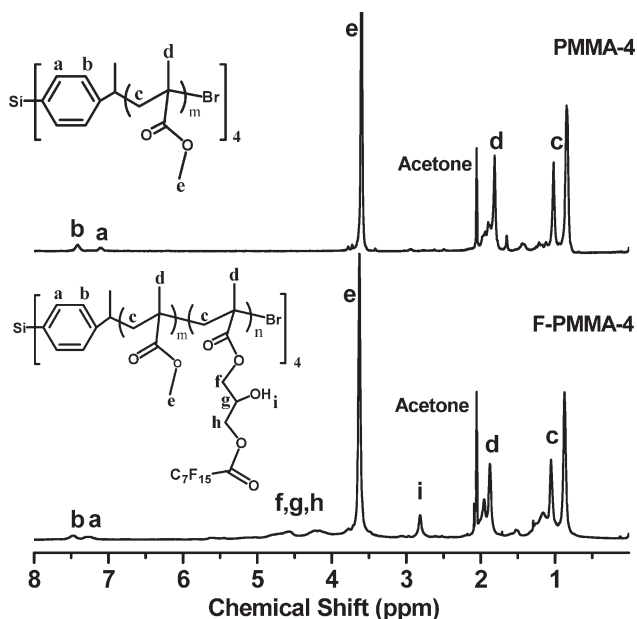


FIGURE 2 ^1H NMR spectra of star-shaped PMMA macroinitiator (PMMA-4) and PMMA-*b*-Poly(FGOA) copolymer (F-PMMA-4).

for the star-shaped PMMA macroinitiators are presented in Table 1. Their M_n values are in the range from 6800 to 25,000 g/mol.

In addition, the polymerization kinetics of MMA monomer initiated by BTES was studied by plotting the monomer conversion ($\ln([M]_0/[M]_t)$) against the polymerization time at 30 °C (Fig. 3). The samples were obtained under the same polymerization conditions with different polymerization time. The ratio of $[I]_0:[\text{Cu(I)Br}]_0:[\text{PMDETA}]_0:[M]_0$ is 1:4:8:400, where $[I]_0$, $[\text{Cu(I)Br}]_0$, $[\text{PMDETA}]_0$, and $[M]_0$ refer to the charged molar concentrations of BETS, Cu(I)Br, PMDETA, and MMA monomer, respectively, while $[M]_t$ is the remaining molar concentrations of MMA monomer at time t . As shown in Figure 3, the variation of $\ln([M]_0/[M]_t)$ with polymerization time follows a good linear relationship. Therefore, the concentration of the propagating radicals in the system is constant and the kinetics obey a first-order dependence on $[M]_0$, indicative of a controlled-manner polymerization.

TABLE 1 Molecular Weights and Distributions of Star-Shaped PMMA Macroinitiators

Sample	^1H NMR		GPC		
	M_n (kg/mol)	$\text{DP}_{\text{PMMA}}^a$	M_n (kg/mol)	M_w (kg/mol)	M_w/M_n
PMMA-1	24.9	60.39	44.5	49.5	1.13
PMMA-2	15.4	36.43	34.0	38.2	1.12
PMMA-3	14.1	33.38	25.3	29.9	1.18
PMMA-4	6.8	15.14	12.9	16.0	1.24

^a Number averaged polymerization degree of PMMA arm.

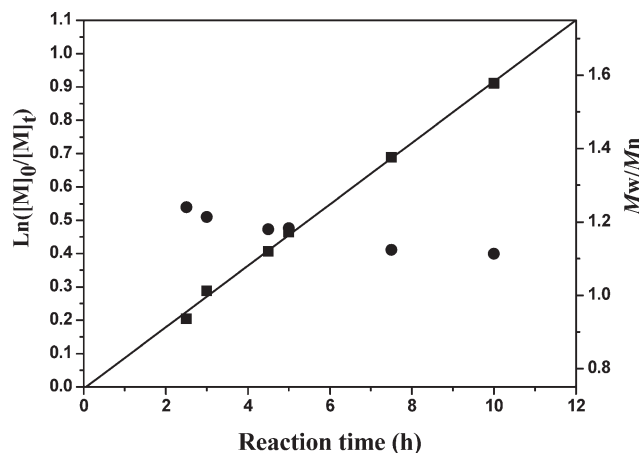


FIGURE 3 Dependence of $\ln([M]_0/[M]_t)$ and M_w/M_n on polymerization time of MMA at 30 °C using BTES as initiator with $[M]_0:[I]_0:[\text{CuBr}]_0:[\text{PMDETA}]_0 = 400:1:4:8$.

The GPC traces of bromo-terminated star-shaped PMMA macroinitiators are illustrated in Figure 4, which are monomodal with the relatively low polydispersity indices ranging from 1.12 to 1.24 (Table 1), reflecting the well-controlled polymerization characteristic. On the other hand, it is seen that the data of M_n obtained from GPC are significantly larger than those by ^1H NMR method. This deviation is rational since the number averaged molecular weight derived from GPC is only a relative value to the linear PS standard, whereas the hydrodynamic volumes of star-shaped polymers and are much different from that of linear PS.^{30,31}

Synthesis and Characterization of Star-Shaped Fluorinated Block Copolymers

Four bromo-terminated star-shaped PMMA macroinitiators with different molecular weights were used to continuously initiate the ATRP polymerization of the FGOA, respectively, to generate four star-shaped fluorinated block copolymers

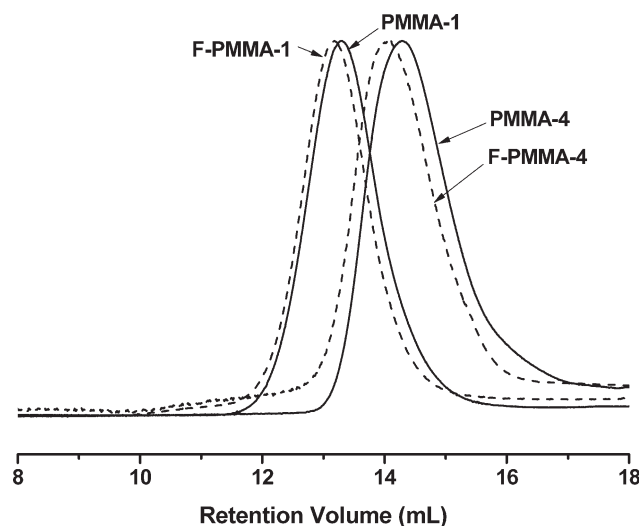


FIGURE 4 GPC curves of star-shaped PMMA macroinitiators and the PMMA-*b*-Poly(FGOA) copolymers.

TABLE 2 Molecular Weights and Distributions of Fluorinated Star-Shaped Block Copolymers

	¹ H NMR			GPC		
	F (wt%)	M _n (kg/mol)	DP _{FGOA} ^a	M _n (g/mol)	M _w (kg/mol)	M _w /M _n
F-PMMA-1	4.16	27.1	1.03	52.0	65.9	1.27
F-PMMA-2	10.3	19.4	1.82	38.3	44.1	1.12
F-PMMA-3	13.8	19.2	2.27	36.2	47.1	1.30
F-PMMA-4	31.7	16.7	4.44	37.2	44.0	1.18

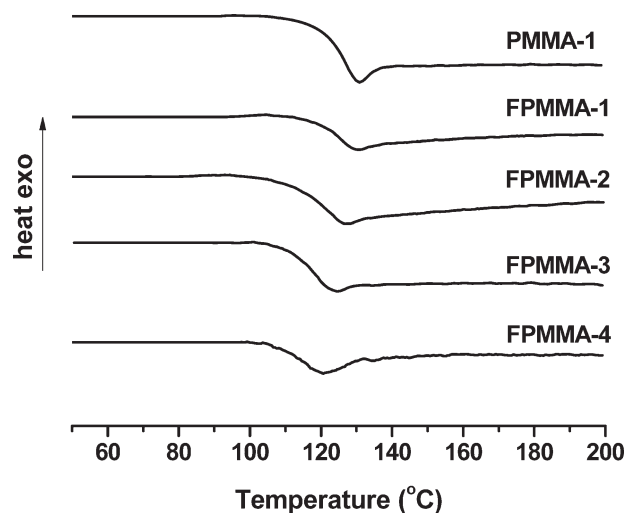
^a Number averaged polymerization degree of poly(FGOA) segment.

PMMA-*b*-poly(FGOA)s (Scheme 1). Compared with the non-fluorinated PMMA-4 sample, the FTIR spectrum of the fluorinated F-PMMA-4 (Supporting Information Fig. S3) shows a new absorption at 1782 cm⁻¹ corresponding to the ester bond of poly(FGOA) segment,²⁶ indicating that FGOA monomer has indeed participated in the copolymerization. The absorption of stretching vibration of C-F bond is overlapped with that of C—O—C linkage, but the band at 1100–1250 cm⁻¹ in F-PMMA-1 sample becomes broadened and enhanced, indicating that FGOA monomer has indeed participated in the copolymerization. The absorption of stretching vibration of C—F bond is overlapped with that of C—O—C linkage, but the band at 1100–1250 cm⁻¹ in F-PMMA-1 sample becomes broadened and enhanced.

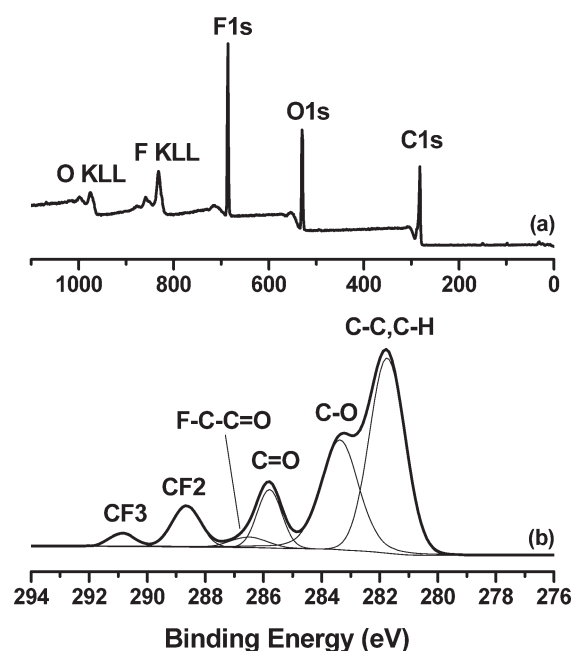
The representative ¹H NMR spectrum of F-PMMA-4 is presented in Figure 2. The peak at 3.68 ppm is attributed to the protons of —OCH₃ group in PMMA segment, whereas the newly emerged peaks at 4.1–5.2 ppm are assigned to the protons of —CH₂CHOHCH₂— linkage in poly(FGOA) segment, and the signal at 2.73 ppm is attributed to the proton of hydroxyl in FGOA unit. Since the number averaged polymerization degrees (DP_n) of PMMA segment in star-shaped macroinitiators have been obtained by ¹H NMR spectra (Table 1), thus, the average number of FGOA unit per arm can be readily calculated according to the ratio of the peak area of —CH₂CHOHCH₂— linkage to that of —OCH₃ group. The DP_ns of poly(FGOA) segment and the number average molecular weights of the copolymers derived from ¹H NMR spectra are presented in (Table 2). As can be seen, the DP_n values of FGOA segment per arm for the four copolymers are 1.03, 1.82, 2.27, and 4.44, respectively. Accordingly, their fluorine contents are in the range from 4.16 to 31.7 wt %.

The GPC traces of the star-shaped fluorinated block copolymers are shown in Figure 4. Relative to the PMMA macroinitiators, the curves of the copolymers apparently shift toward left, indicating the increase of molecular weight. Moreover, all the samples exhibit quite narrow molecular weight distribution with polydispersities in the range from 1.12 to 1.30 (Table 2).

The fluorinated star-shaped copolymers obtained can readily dissolve in most common solvents such as acetone, THF, diox-

**FIGURE 5** DSC thermograms of star-shaped PMMA-*b*-Poly(FGOA) copolymers.

ane, DMF, N,N-dimethylacetamide, and N-methylpyrrolidone, reflecting the typical characteristic of star-shaped polymers. The DSC traces of the star-shaped block copolymers are shown in Figure 5. It is seen that the glass transition temperatures slightly decrease with the increase of fluorine content. The similar phenomena have also been observed for other fluorinated polymers.³² The reason is contributed to that the long fluorinated side groups act to open up that polymer chains to generate large free volume, leading to an increased motion ability of polymer segments.

**FIGURE 6** XPS survey spectrum (a) and high resolution C_{1s} spectrum (b) for F-PMMA-2 film.

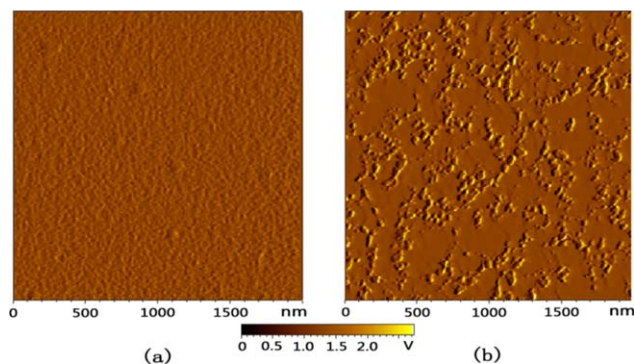


FIGURE 7 AFM images ($2 \times 2 \mu\text{m}^2$) of films for PMMA macroinitiator (a) and F-PMMA-4 (b). [Color figure can be viewed in the online issue, which is available at wileyonlinelibrary.com.]

Hydrophobicity and Optical Properties of Star-Shaped Fluorinated Block Copolymer Films

PMMA is a transparent amorphous thermoplastic material widely employed in a variety of important industrial fields such as the fabrication of optical devices. However, the PMMA chains contain large amount of polar ester groups. The strong hydrophilic nature of PMMA leads to an apparent change of optical parameters upon moving the device to a moisture environment.^{20–23,33} Therefore, its optical stability has to be improved to meet the increasing property requirement in optical applications. The introduction of highly hydrophobic fluorinated groups can be an effective way to enhance the resistance of PMMA material to corrosion of moisture.

The fluorine information on the surface of fluorinated PMMA films was examined by XPS method. The XPS survey spectrum and high-resolution C_{1s} spectrum of the representative F-PMMA-2 recorded at the takeoff angle of 0° are shown in Figure 6. The peaks at 688, 534, and 283 eV are assigned to the fluorine, oxygen, and carbon elements, respectively. Moreover, in the high-resolution C_{1s} spectrum, the signals of CF_3 and CF_2 groups are found at the binding energies of 293

and 291 eV, respectively. The assignments above are consistent with the previously reports of other fluorinated polymers.^{26,34} In addition, the peak at 290 eV is attributed to carbonyl carbon of ester group adjacent to $(\text{CF}_2)_6\text{CF}_3$ group, whereas that at 288 eV is assigned to the carbonyl carbon of ester group in PMMA segments.²⁶ It is found that the measured F/C atomic ratios are significantly higher than the theoretical values according to the charged amount of fluorinated monomer in the polymerization system. For example, the theoretical F/C ratio in FPMMA-2 is 0.126, whereas the measured value calculated from the peak areas of fluorine and carbon signals is as high as 0.324, increased by about 1.9-fold, indicating that the fluorinated segments have quite strong segregation ability from the bulk to the surface. The highly hydrophobic fluorinated groups act as an effective shield against the absorption of water molecules on the polymer films.

AFM measurements for star-shaped non-fluorinated and fluorinated PMMA films were performed in tapping mode to investigate the variation of surface morphology and directly observe the aggregated fluorinated segments on the topmost surface. As shown in Figure 7, the surface of nonfluorinated PMMA film is very smooth and homogeneous. However, with the introduction of fluorine, large amounts of domains appear on the AFM image. The similar images have also been observed in other fluorinated polymer films.^{26,35,36} Taking account of the XPS results, it is deduced that these domains are due to the aggregation of fluorinated groups on the surface.

The effect of fluorine on the hydrophobicity of the polymer films was studied by the measurements of water contact angle (θ). The surface tensions γ_{sv} of the films were calculated by one-liquid method according to the eq 3:³⁷

$$1 + \cos \theta = 2 \sqrt{\frac{\gamma_{sv}}{\gamma_{lv}}} e^{-\beta(\gamma_{lv} - \gamma_{sv})^2} \quad (3)$$

where β is an empirical parameter and is $0.0001247 (\text{mN/m})^{-2}$, while γ_{sv} and γ_{lv} denote the tensions of the solid-air and liquid-air interfaces, respectively. θ is the contact angle of liquid.

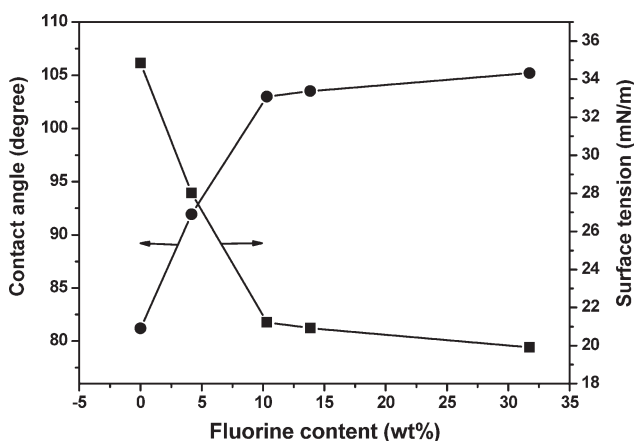


FIGURE 8 Plots of contact angles of water and surface tensions as a function of fluorine content of copolymer films.

TABLE 3 Refractive Indices and Birefringences of Star-Shaped Copolymer Films

Sample	Wavelength (1310 nm)			Wavelength (1550 nm)		
	n_{TE}	n_{TM}	Δn^a	n_{TE}	n_{TM}	Δn^a
PMMA-1	1.4763	1.4758	0.0005	1.4753	1.4753	0.0001
F-PMMA-1	1.4737	1.4734	0.0003	1.4721	1.4721	0.0000
F-PMMA-2	1.4715	1.4713	0.0002	1.4699	1.4700	0.0001
F-PMMA-3	1.4708	1.4708	0.0000	1.4694	1.4693	0.0000
F-PMMA-4	1.4619	1.4615	0.0004	1.4609	1.4609	0.0000

^a Birefringence, $\Delta n = n_{TE} - n_{TM}$.

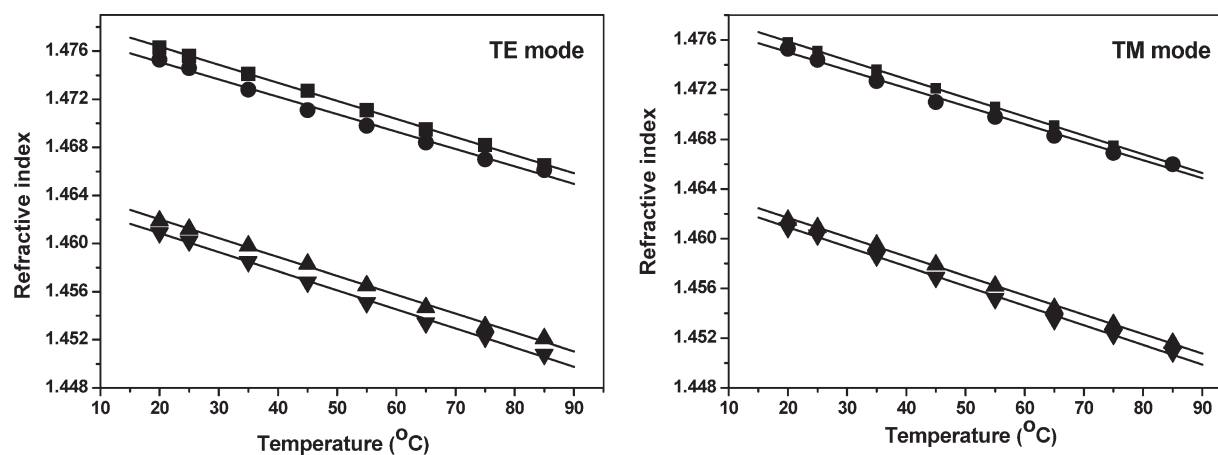


FIGURE 9 Refractive index versus temperature at TE mode and TM mode for (■) PMMA-1 at 1310 nm; (●) PMMA-1 at 1550 nm; (▲) F-PMMA-4 at 1310 nm; (▼) F-PMMA-4 at 1550 nm.

The results in Figure 8 show that the fluorinated star-shaped polymers exhibit remarkably enhanced hydrophobicity. For example, the water contact angle of the non-fluorinated film is only 81° . With the introduction of fluorine, the θ value remarkably increases to 105° . Correspondingly, the surface tensions γ_{sv} of the fluorinated samples decrease from 34.8 to 19.9 mN/m. The improved hydrophobicity is favorable for the optical stability when the optical devices are moved from dry to wet environment. In addition, it is found that, when the fluorine content exceeds 10 wt %, the increase of contact angles and decrease of γ_{sv} values with fluorine content become rather slow, implying that the enrichment of fluorine on the surface has approached saturation. Thus, for the star-shaped PMMA polymers, the excellent hydrophobicity can be achieved by the incorporation of small amount of fluorine. This property is also desirable for the practical application based on the cost-saving consideration since the fluorinated monomers are usually very expensive.

The refractive indices, birefringences, and thermo-optic coefficients of the star-shaped polymer films were measured with a prism coupler at 1310 and 1550 nm, which wavelengths are the most common used for optical communications. The data in Table 3 show that the refractive indices of the fluorinated star-shaped copolymers range from 1.4763 to 1.4619 with the incremental fluorine content, indicating that refractive index of these copolymers can be tuned and controlled through variations of the length of poly(FGOA) segments.

Birefringence refer to the difference between the refractive indices at TE and TM modes ($\Delta n = n_{TE} - n_{TM}$), which reflects the optical anisotropy of a material. Low birefringence is required for optical communications in order to reduce polarization dependent loss.³⁸ In this work, the designed polymers have star-shaped topology with a rigid and bulky tetraphenylsilane core which is expected to effectively hinder the orientation of polymer chains or segments along the surface of substrate, and thereby decrease the bire-

fringence of polymer films. Indeed, as shown in Table 3, the birefringence coefficients of all the polymers at 1310 nm are <0.0005 . Surprisingly, it is found that their birefringence coefficients at 1550 nm are close to zero, which are even lower than the measurement accuracy of the prism coupler employed.

However, the refractive indices of polymer films at different temperatures from 20 to 85 °C are also measured. For both the nonfluorinated and fluorinated polymers, the relationship between refractive indices and temperatures exhibit good straight lines (Fig. 9). From the slopes of lines the thermo-optical coefficients of polymer films were calculated, and the data are listed in Table S1 (Supporting Information). It is seen that the absolute values of the thermo-optical coefficients of polymer films are in the range from 1.44×10^{-4} to 1.59×10^{-4} , which are about a magnitude order larger than that of inorganic materials.³⁸ In addition, it is noted that the absolute values of the thermo-optical coefficients exhibit a growing trend with the increase of fluorine content. For polymer materials, the thermal-optical coefficient is proportional to volume coefficient of thermal expansions (α),³⁹ whereas the α value is positively correlated to the free volume of polymer. As mentioned in the discussion of glass transition temperature, for the fluorinated star-shaped polymers, the long fluorinated side groups act to open up that polymer chains to generate large free volume. Therefore, the end-capping of star-shaped PMMA with poly(FGOA) segments leads to an increased thermo-optical coefficients. High thermo-optic coefficients of polymer films are important for applications in the active optical switches and wavelength filter devices.

CONCLUSIONS

In this work, a tetrafunctional ATRP initiator, BTES, was synthesized and characterized. Then, in the presence of CuBr/PMDETA, BTES was used to initiate the ATRP of MMA to generate bromine-terminated star-shaped four-armed PMMA macroinitiator, which further initiated polymerization of FGOA to create

novel star-shaped fluorinated block copolymers PMMA-*b*-poly(FGOA)s with narrow molecular weight distributions (≤ 1.30) and varied fluorine contents from 0 to 31.7 wt%. The fluorinated copolymers exhibit excellent solubility in common organic solvent and good film-formation. The fluorine information, morphology, and hydrophobicity of film surface were investigated by the measurements of XPS, AFM, water contact angle, and calculation of surface tension. It is found that the surface tensions of polymer films remarkably decrease from 34.8 to 19.9 mN/m after end-capping of the arms with fluorinated segments. The copolymer films have adjustable refractive indices over a range of 1.4619–1.4763, and extremely low birefringences. In addition, they show quite high thermo-optic coefficients of around $1.5 \times 10^{-4} \text{C}^{-1}$, exhibiting the advantage in decreasing the power consumption and the application in optical switch devices.

ACKNOWLEDGMENTS

The authors thank the National Science Foundation of China (No. 51273031, 51473026 and U1462125) for financial support of this research. They are grateful to Professor Mingshan Zhao (School of Physics & Optoelectronic Engineering, Dalian University of Technology) for the help of measurements of optical properties of films.

REFERENCES AND NOTES

- 1 K. Matyjaszewski, N. V. Tsarevsky, *Nat. Chem.* **2009**, *1*, 276–288.
- 2 H. Kudo, H. Inoue, T. Inagaki, T. Nishikubo, *Macromolecules* **2009**, *42*, 1051–1057.
- 3 C. Ventura, P. Thornton, S. Giordani, A. Heise, *Polym. Chem.* **2014**, *5*, 6318–6324.
- 4 X. S. Feng, C. Y. Pan, *Macromolecules* **2002**, *35*, 2084–2089.
- 5 G. H. Deng, Y. M. Chen, *Macromolecules* **2004**, *37*, 18–26.
- 6 H. J. Zhang, Q. Yan, Y. Kang, L. L. Zhou, H. Zhou, J. Y. Yuan, S. Z. Wu, *Polymer* **2012**, *53*, 3719–3725.
- 7 A. Dworak, A. Kowalczyk, B. Mendrek, B. Trzebicka, *Macromol. Symp.* **2011**, *308*, 93–100.
- 8 A. Kurt, K. A. Demirelli, *Polym. Eng. Sci.* **2010**, *50*, 268–277.
- 9 Y. H. So, S. F. Hahn, Y. F. Li, M. T. Reinhard, *J. Polym. Sci. Part A: Polym. Chem.* **2008**, *46*, 2799–2806.
- 10 T. Liu, X. J. Li, Y. F. Qian, X. L. Hu, S. Y. Liu, *Biomaterials* **2012**, *33*, 2521–2531.
- 11 F. J. Xu, Z. X. Zhang, Y. Ping, J. Li, E. T. Kang, K. G. Neoh, *Biomacromolecules* **2009**, *10*, 285–293.
- 12 Y. F. Tong, L. Chen, X. H. He, Y. W. Chen, *J. Polym. Sci. Part A: Polym. Chem.* **2013**, *51*, 4341–4350.
- 13 X. Y. Huan, D. L. Wang, R. Dong, C. L. Tu, B. S. Zhu, D. Y. Yan, X. Y. Zhu, *Macromolecule* **2012**, *45*, 5941–5947.
- 14 J. L. Pan, Z. Li, L. F. Zhang, Z. P. Cheng, X. L. Zhu, *Chin. J. Polym. Sci.* **2014**, *32*, 1010–1018.
- 15 A. Hirao, K. Kawasaki, T. Higashihara, *Macromolecules* **2004**, *37*, 5179–5189.
- 16 F. Sanda, H. Sanada, Y. Shibasaki, T. Endo, *Macromolecules* **2002**, *35*, 680–683.
- 17 W. A. Zhang, A. H. E. Müller, *Macromolecules* **2011**, *43*, 3148–3152.
- 18 P. Polanowski, J. L. Jeszka, K. Matyjaszewski, *Polymer* **2014**, *55*, 2552–2561.
- 19 Y. Gnanou, D. Taton, *Macromol. Symp.* **2001**, *174*, 333–341.
- 20 Z. Zhang, Z. G. Xiao, J. R. Liu, C. P. Grover, *Fiber Integr. Opt.* **2003**, *22*, 343–355.
- 21 T. Watanabe, N. Ooba, Y. Hida, M. Hikita, *Appl. Phys. Lett.* **1998**, *72*, 1533–1535.
- 22 G. Hanisch, P. R. Podgorsek, H. Franke, *Sens. Actuators B* **1998**, *51*, 348–354.
- 23 M. P. Pakhomov, I. Zubkov, D. S. Khizhnyak, *ACS Symp. Ser.* **2001**, *795*, 177–194.
- 24 J. Scheirs, *Modern Fluoropolymers*; Wiley: New York, **1997**.
- 25 Z. J. Wang, M. Maric, *J. Polym. Sci. Part A: Polym. Chem.* **2013**, *51*, 2970–2978.
- 26 Y. B. Cheng, Z. G. Wang, *Polymer* **2013**, *54*, 3047–3054.
- 27 A. C. Terraza, H. L. Tagle, H. J. Lembach, *Chil. Chem. Soc.* **2010**, *55*, 137–140.
- 28 H. K. Kim, M. K. Ryu, S. M. Lee, *Macromolecules* **1997**, *30*, 1236–1239.
- 29 Y. Q. Xu, Q. F. Xu, J. M. Lu, X. W. Xia, L. H. Wang, *Eur. Polym. J.* **2007**, *43*, 2028–2034.
- 30 E. Martinelli, G. Galli, S. Krishnan, Y. M. Paik, K. C. Ober, A. D. Fischer, *J. Mater. Chem.* **2011**, *21*, 15357–15368.
- 31 P. Moschogianni, S. Pispas, N. J. Hadjichristidis, *Polym. Sci. Polym. Chem.* **2001**, *39*, 650–655.
- 32 V. Darras, O. Fichet, F. Perrot, S. Boileau, D. Teyssié, *Polymer* **2007**, *48*, 687–695.
- 33 J. Yoshida, Y. Kawabe, N. Ogata, *Proc. SPIE* **2010**, *765*, 1–8.
- 34 X. J. Cui, S. L. Zhong, Y. Gao, H. Y. Wang, *Colloid Surf A: Physicochem. Eng. Asp.* **2008**, *324*, 14–21.
- 35 W. Ming, X. W. Lou, R. D. Grampel, J. L. J. Dongen, R. Linde, *Macromolecules* **2001**, *34*, 2389–2393.
- 36 W. Ming, M. Tian, R. D. Grampel, F. Melis, X. Jia, J. Loos, R. Linde, *Macromolecules* **2002**, *35*, 6920–6929.
- 37 D. Y. Kwok, C. J. Budziak, A. W. Neumann, *J. Colloid Interface Sci.* **1995**, *173*, 143–150.
- 38 V. Raghunathan, J. L. Yagüe, J. J. Xu, J. Michel, K. K. Gleason, C. L. Kimerling, *Opt. Express* **2012**, *20*, 20808–20813.
- 39 Z. Zhang, P. Zhao, P. Lin, F. T. Sun, *Polymer* **2006**, *47*, 4893–4896.